Available online at website: https://journal.bcrec.id/index.php/bcrec

Bulletin of Chemical Reaction Engineering & Catalysis, 22 (1) 2027, 69-87

Original Research Article

Box-Behnken Design Optimization of Eco-Friendly Walnut Shell-Derived Activated Carbon for Enhanced Paracetamol Adsorption

Mariem Ouled Mohamed[1], Leila Khalfa[1,2], Noureddine Hamdi[3]*, Walid Maherzi[4], Mohamed Bagane[1]

[1]Applied Thermodynamic Laboratory, National School of Engineers of Gabès (ENIG), University of Gabes, 6072, Zrig, Tunisia.
[2]National School of Engineers of Gafsa (ENIGA), University of Gafsa, 2112, Tunisia.
[3]Higher Institute of Water Sciences and Techniques, University of Gabes, 6072, Zrig, Tunisia, Laboratory of Composite Materials and Clay Minerals, National Center for Research in Material Sciences (CNRSM), 8020, Soliman, Bordj Cedria, Tunisia.
[4]Department of Civil Engineering and Environmental, IMT Lille Douai, EA 4515 - 10 LGCgE, University of Lille, F-59000 Lille, France.

Received: 16th September 2026; Revised: 21th October 2026; Accepted: 26th October 2026
Available online: 6th November 2026; Published regularly: April 2027

Abstract

In this work, a low-cost activated carbon derived from walnut shells (WSAC) was developed through pyrolysis coupled with chemical activation using $ZnCl_2$. The preparation process was statistically optimized using the Box–Behnken design (BBD) to assess the influence of impregnation ratio, carbonization time, and carbonization temperature on the textural properties of the material. The optimal conditions, predicted by Design Expert, corresponded to a carbonization temperature of 450 °C, a carbonization time of 90 min, and an impregnation ratio of 1:1 (w/w). Under these conditions, the WSAC achieved a high specific surface area of 873 m^2/g and a total pore volume of 0.490 cm^3/g, indicating a predominantly mesoporous structure. The physico-chemical properties of WSAC, including thermogravimetric analysis, crystalline structure, morphology, functional groups, and surface area, were investigated using various techniques such as TGA-DTG, SEM, XRD, FTIR, pH_{ZPC}, and BET analysis. The adsorption behavior of paracetamol (PCT) from aqueous solution was systematically evaluated as a model pharmaceutical contaminant. The effects of solution pH, temperature, initial concentration, and adsorbent dosage were investigated. The adsorption data were best described by the Langmuir isotherm, with a maximum monolayer adsorption capacity of 62.06 $mg.g^{-1}$, while the kinetic results followed a pseudo-second-order model ($R^2 = 0.999$). It was found that the adsorption mechanism involves hydrogen bonding and π–π interactions. Thermodynamic parameters revealed that the adsorption process is spontaneous and exothermic. These results show that WSACs can be an efficient adsorbent for the removal of PCT or other pharmaceutical pollutants from water.

Copyright © 2027 by Authors, Published by BCREC Publishing Group. This is an open access article under the CC BY-SA License (https://creativecommons.org/licenses/by-sa/4.0).

Keywords: Walnut shell; activated carbon; Optimization; Box-Behnken design; PCT adsorption

How to Cite: Ouled Mohamed, M., Khalfa, L., Hamdi, N., Maherzi, W., Bagane, M. (2027). Box-Behnken Design Optimization of Eco-Friendly Walnut Shell-Derived Activated Carbon for Enhanced Paracetamol Adsorption. *Bulletin of Chemical Reaction Engineering & Catalysis*, 22 (1), 69-87. (DOI: 10.9767/bcrec.20857)

Permalink/DOI: https://doi.org/10.9767/bcrec.20857

1. Introduction

In recent years, the continuous discharge of pharmaceutical compounds into water sources has emerged as a critical environmental issue worldwide. These micropollutants, which come from industrial, hospital, and residential wastewater, are frequently resistant to traditional treatment methods and are continuously released into water bodies [1].

The pharmaceutical most commonly detected in surface water, groundwater, and wastewater is paracetamol [2]. This compound is a non-steroidal anti-inflammatory drug and is present in numerous medicines. Given their functions for

* Corresponding Authors.
Email: nouryhamdi@gmail.com (N. Hamdi)

pain relief and fever reduction, these medications are among the most utilized globally, thus constituting pervasive environmental contaminants [3]. It has been noted that the world production of paracetamol is around 145,000 tons annually. Additionally, it is readily accessible in numerous countries and it can be bought without a prescription; thus, its consumption is excessively occurring [4]. However, excessive or prolonged exposure to PCT can lead to adverse health effects, including digestive disorders, diarrhea, and stomach cancer [2]. Furthermore, even at low concentrations, PCT has a toxic effect on organisms living in both aquatic and terrestrial environments [5]. Therefore, it is important to develop effective and affordable technologies to remove PCT from wastewater before its discharge into the environment.

Currently, many technologies of water treatment have been applied for the removal of paracetamol, including aerobic degradation [6], fenton-based processes [7,8], membrane processes [9], like electrolysis [10] and nanofiltration [11–13], photocatalytic ozonation [14,15], and ion exchange [16]. However, these technologies are generally costly, can be generate harmful by-products, and do not sufficiently fulfill such discharge requirements. In the last decades, adsorption has been regarded as a promising method for PCT removal due to its simplicity, high efficiency, and eco-friendliness. In this regard, it is consistently recommended to use low-cost and biodegradable materials adsorbents. Indeed, the most commonly used adsorbents for PCT adsorption include natural clay [69], silica gel [18], zeolite [19], nanocomposite [20], and biochar [21]. However, the activated carbon stands out as the most effective adsorbents, due to its paramount properties, such as a high surface area, porous structure, regeneration possibility, and the ability to remove many contaminants selectively [22–25].

This study focuses on the synthesis and optimization of activated carbon derived from walnut shells (WSAC) for the efficient adsorption of paracetamol from aqueous media. The preparation conditions were optimized using Response Surface Methodology (RSM) based on the Box– Behnken design (BBD). The response surface methodology stands out for its many advantages. Firstly, it minimizes the number of requisite experiments. Secondly, the methodology incorporates analysis of variance (ANOVA) to verify the precision and statistical robustness of the obtained results. Thirdly, it enables the assessment of both individual factors and their synergistic interactions, providing a comprehensive understanding of their effects. Lastly, RSM also employs 3D surface plots to visualize variable effects, facilitating the interpretation of complex interactions. Furthermore, the influence of process variables such as solution pH, temperature, initial paracetamol concentration, and adsorbent dosage on adsorption performance was systematically investigated. Kinetic, isothermal, and thermodynamic studies were conducted to elucidate the adsorption mechanism and evaluate the spontaneity and nature of the process. Overall, this work highlights the potential of walnut shell biomass as a sustainable, low-cost precursor for high-performance activated carbon and advances the development of an effective adsorbent for the removal of pharmaceutical contaminants from water.

2. Materials and Methods

2.1 Materials

Walnut shells, sourced locally from Tunisia, were used as the biomass precursor for the synthesis of the activated carbon. Chemical activation was performed using zinc chloride ($ZnCl_2$, 98% purity) as the activating agent. Paracetamol ($C_8H_9NO_2$) was selected as the target pollutant for the adsorption studies. All other reagents used in this work, including hydrochloric acid (HCl), sodium hydroxide (NaOH), sodium chloride (NaCl), and potassium bromide (KBr), were of analytical grade and were used as received without further purification.

2.2. Synthesis of Walnut Shell-Derived Activated Carbon

The initial preparation of the raw material involved thorough washing with distilled water to eliminate any surface dust and inorganic contaminants. The washed precursor was then air dried at ambient temperature for 48 hours to minimize its residual moisture content. Subsequently, the dried material was crushed and sieved to obtain a uniform particle size fraction within the 1 to 2 mm range. The elemental analysis of the final prepared precursor is detailed in Table 1 [26].

Table 1. Elemental analysis of walnut shells.

Sample	Elemental analysis (wt.%)				
	C	O	H	N	S
Walnut shell	47.74	45.61	6.03	0.40	0.22

Copyright © 2027, ISSN 1978-2993

To efficiently optimize the activation and carbonization parameters while minimizing the number of experimental trials, a Box-Behnken design (BBD) with three factors and three center-point replicates was applied. The total number of runs was calculated as $N = 2k(k - 1) + C_0$, where k is the number of factors and C_0 is the number of center-point replicates, giving 15 experiments. The three independent variables investigated were the impregnation ratio, the carbonization time, and the carbonization temperature. The sample was chemically activated with zinc chloride ($ZnCl_2$) at an impregnation ratio of (1–2 w/w). It was then pyrolyzed at a temperature range of (350–550 °C), using a heating rate of 10 °C/min and residence times of (30–90 min) under a nitrogen atmosphere. Afterwards, the impregnated material was rinsed with hot distilled water to remove excess zinc chloride until reaching a pH of 6-7, and finally dried in an oven at 80 °C for 24 h.

2.3. Experimental design

In this work, response surface methodology (RSM) based on a Box-Behnken design (BBD) was used to investigate the effects of three independent variables, namely impregnation ratio (*A*), carbonization time (*B*), and carbonization temperature (*C*), on the BET surface area (S_{BET}) and total pore volume (V_P) of the activated carbon. Table 2 lists the experimental ranges of the independent variables together with their coded levels.

Design-Expert software (version 13) was used to generate the experimental design and analyze the data. The relationship between each response and the independent variables was described by an empirical second-order polynomial model (Equation (1)). The influence of the operating factors was evaluated through analysis of variance (ANOVA) and the coefficient of determination (R^2). The F-values were used to test the adequacy of the models, while the p-values were used to assess the significance of each model term.

$$Y = b_0 + b_1 \times A + b_2 \times B + b_3 \times C + b_{11} \times A^2 + b_{22} \times B^2 + b_{33} \times C^2 + b_{12} \times AB + b_{13} \times AC + b_{23} \times BC \quad (1)$$

Where Y is the predicted response, b_0 is the constant coefficient, (b_1, b_2 and b_3) are the linear coefficients, (b_{11}, b_{22} and b_{33}) are the quadratic coefficients, (b_{12}, b_{13} and b_{23}) are the interaction coefficients, and A, B, C are the independent variables.

2.4. Characterizations Techniques

Several characterization techniques have been applied to analyze the properties of the optimum activated carbon and the precursor. Thermal analysis (TGA/DTG) was carried out from 25 to 1000 °C at a heating rate of 10 °C min^{-1}. The surface area and pore volume of the material were determined using the BET (Brunauer–Emmett–Teller) method through nitrogen adsorption–desorption isotherms at 77 K on a Micromeritics 3 Flex analyzer. X-ray diffraction (XRD, D2 PHASER, Bruker) was employed to examine the crystal structure of the material. Morphology and particle size were investigated using scanning electron microscopy (SEM, JEOL JCM-7000). Fourier-transform infrared spectroscopy (FT-IR, Thermo-Fisher) was performed with KBr pellets over the 4000-400 cm^{-1} range to identify surface functional groups. The zero-point charge (pH_{ZPC}) of the materials was determined using the pH drift method described by Rawat et al. [27]. Finally, the concentration of paracetamol was quantified using a UV–VIS spectrophotometer (PG Instruments T80) at a wavelength of 242.5 nm.

2.5. Adsorption experiments

In this study, the paracetamol adsorption experiment was conducted in batch mode. Various operational parameters were examined, including the solution pH (3 to 12), the adsorbent dose (0.4 to 3 $g.L^{-1}$), and the initial PCT concentration (20 to 50 $mg.L^{-1}$). The adsorption isotherms were analyzed to gather detailed information on the adsorption process efficiency. Additionally, the solution temperature varied between 308 and 338 K to determine the thermodynamic parameters associated with the adsorption process.

The removal efficiency R (%) and adsorption capacity q_e ($mg.g^{-1}$) of this activated carbon were computed according to the following expressions: Equations (2) and (3).

Table 2. Independent variables and their coded levels.

Factors	Code	Unit	Coded variables levels	
			-1	+1
Impregnation ratio	A	w/w	1	2
Time carbonization	B	min	30	90
Carbonization temperature	C	°C	350	550

Copyright © 2027, ISSN 1978-2993

$$R = \frac{C_0 - C_e}{C_0} \times 100\% \quad (2)$$

$$q_e = \frac{(C_0 - C_e) \times V}{W} \quad (3)$$

where C_0 and C_e are the initial and equilibrium concentrations of paracetamol (mg.L^{-1}), V is the volume of solution (L), and W is the mass of activated carbon (g).

2.6. Analytical Methods

The residual PCT concentration was measured at 242.5 nm with a PG Instruments T80 UV-VIS spectrophotometer, after filtering each sample through a 0.45 µm syringe filter to remove the adsorbent particles. All experiments were performed in triplicate, and the results are expressed as mean values, with a relative error of about 3%.

2.7. Adsorption Kinetics

The study of adsorption kinetics describes the rate at which a solute is adsorbed and the contact time required between the adsorbent and adsorbate to reach a steady state or pseudo-equilibrium in the system [28]. This knowledge is of considerable practical significance, as it can help save both time and energy. The pseudo first order (PFO), pseudo second order (PSO), and intraparticle diffusion (IPD) kinetic models are commonly employed to investigate adsorption processes in aqueous solutions [29].

The PFO kinetic model (Equation 4) is written as:

$$q_t = q_e (1 - e^{-K_1 t}) \quad (4)$$

Where q_e and q_t are the amounts adsorbed at equilibrium and at time t respectively, (mg.g^{-1}) and K_1 is the PFO model's rate constant (min^{-1}). The PSO kinetic rate (Equation 5) is expressed as follows:

$$q_t = \frac{q_e^2 K_2 t}{1 + q_e K_2 t} \quad (5)$$

where K_2 corresponds to the pseudo-second-order rate constant (g.mg^{-1}.min^{-1}). The IPD model is expressed by the following equation (Equation 6):

$$q_t = K_{id} t^{\frac{1}{2}} + C_i \quad (6)$$

where K_{id} is the intraparticle diffusion rate constant, (mg.g^{-1}.min$^{-1/2}$), and C_i is a constant related to the boundary layer thickness, (mg.g^{-1}).

2.8. Adsorption Isotherms

Adsorption isotherms illustrate the interaction between the adsorbent and the contaminant. They are widely used to evaluate adsorption capacity, the affinity of the adsorbent, the performance of the adsorption system, and the underlying adsorption mechanism. Several isotherm models exist, with the most common being the Langmuir single layer and the Freundlich multilayer adsorption models.

The Langmuir isotherm assumes that adsorption occurs as a monolayer on a homogeneous surface, with constant enthalpy and sorption activation energy. Equation (7) expresses the nonlinear form of the Langmuir model.

$$q_e = \frac{q_m K_l C_e}{1 + K_l C_e} \quad (7)$$

where q_e is the quantity of paracetamol adsorbed (mg.g^{-1}), C_e is the equilibrium PCT concentration (mg.L^{-1}), K_L is a Langmuir constant (L/mg), and q_m is the maximun adsorption capacity (mg.g^{-1}). A dimensionless constant (R_L) also can be added (Equation 8).

$$R_L = \frac{1}{1 + K_L C_0} \quad (8)$$

The value of the separation factor makes it possible to characterize the nature of the adsorption process: it is considered unfavorable when $R_L > 1$, linear when $R_L = 1$, favorable when $0 < R_L < 1$, and irreversible when $R_L = 0$.

The Freundlich isotherm is an empirical model used to describe heterogeneous systems. It can be described by Equation 9.

$$q_e = K_f C_e^{\frac{1}{n}} \quad (9)$$

where K_f is a Freundlich constant (mg$^{1-1/n}$.L$^{1/n}$.g^{-1}) and n is the adsorption intensity.

To evaluate how well the theoretical adsorption models fit the experimental data, three commonly reported error functions were calculated: the sum of squared errors (SSE), the root mean square error (RMSE), and the chi-square (χ^2). These error functions are expressed by the following equations:

$$ESS = \sum_{i=1}^{n} (q_{e,exp} - q_{e,cal})^2 \quad (10)$$

$$RMSE = \sqrt{\frac{1}{n} \sum_{i=1}^{n} (q_{e,exp} - q_{e,cal})^2} \quad (11)$$

$$\chi^2 = \sum_{i=1}^{n} \frac{(q_{e,exp} - q_{e,cal})^2}{q_{e,cal}} \quad (12)$$

where $q_{e,exp}$ and $q_{e,cal}$ are the experimental and calculated adsorption capacities at equilibrium (mg.g^{-1}), respectively, and n is the number of experimental data points.

2.9. Thermodynamic Studies

Thermodynamic studies are carried out to determine the spontaneity of a reaction and its endothermic or exothermic nature. The

Copyright © 2027, ISSN 1978-2993

thermodynamic equations were computed using the following expressions (Equations 13 and 14):

$$\Delta G° = -RT \ln K_d \quad (13)$$
$$\Delta G° = \Delta H° - \Delta S° \quad (14)$$

where $\Delta G°$, $\Delta S°$, and $\Delta H°$ represent the Gibbs free energy, entropy change, and enthalpy change respectively. R is the universal gas constant (8.314 J/mol.K), T is the absolute temperature (K), and k_d is the thermodynamic equilibrium constant calculated by Equation 15, with $K_d = \frac{q_e}{C_e}$.

$$\ln K_d = \frac{\Delta S°}{R} - \frac{\Delta H°}{RT} \quad (15)$$

3. Results and Discussion

3.1. Optimization of Process for Production of Activated Carbon from Walnut Shell

The study investigated the correlations between the BET surface area, total pore volume, and three independent variables: impregnation ratio (A), carbonization time (B), and carbonization temperature (C). Table 3 presents the results for S_{BET} and V_P for each experimental run. The outcomes show the specific surface area ranged from 224 to 876 m²/g, while the total pore volume was in the range of 0.13-0.496 cm³/g.

The experimental results were fitted to a quadratic model, and the final equations in terms of coded factors are given in Equations (16) and (17) for S_{BET} (Y_1) and V_p (Y_2), respectively.

$$S_{BET}\ (m^2/g) = 401.445 + 120.892\ C - 70.944\ AB + 138.708\ A^2 + 179.192\ B^2 - 143.826\ C^2 \quad (16)$$

$$V_P\ (cm^3/g) = 0.236 + 0.066\ C - 0.044\ AB + 0.071\ A^2 + 0.096\ B^2 - 0.088\ C^2 \quad (17)$$

Synergistic and antagonistic effects on the response are indicated by positive and negative signs, respectively [30,31]. Regression equations (16) and (17) indicate that carbonization temperature has a significant linear effect on both the BET surface area and total pore volume of the activated carbon. Additionally, the interaction between carbonization time and impregnation ratio was found to be significant. Quadratic effects of the impregnation ratio, carbonization time, and carbonization temperature were also significant.

Analysis of Variance (ANOVA) is a fundamental statistical technique used to identify the sources of variation in data. It is employed to determine the most significant factors and their interactions. Additionally, ANOVA can evaluate the reliability of a model [32]. To assess the adequacy of the proposed model in fitting the experimental data, parameters such as R², F-value, p-value, and lack of fit were analyzed [33,34]. The results of the ANOVA for the response models of BET surface area and total pore volume are presented in Tables 4 and 5, respectively.

The ANOVA results show that the model F-values for S_{BET} and V_P were 21.13 and 18.32, respectively, indicating that the quadratic models are statistically significant for both responses. The non-significant lack of fit further confirms that the models adequately represent the experimental data. The coefficients of determination (R² = 0.9744 for S_{BET} and 0.9706 for V_P) and the adjusted R² values (0.9283 and 0.9176,

Table 3. Experimental design matrix and responses.

Run	Activated carbon preparation variables			Responses	
	Impregnation ratio (w/w)	Carbonization Temperature (°C)	Carbonization time (min)	BET surface (m²/g)	Total pore volume (cm³/g)
1	1	350	60	324	0.18
2	1	550	60	441	0.24
3	2	350	60	263	0.15
4	2	550	60	556	0.31
5	1.5	350	30	224	0.13
6	1.5	550	30	623	0.34
7	1.5	350	90	371	0.21
8	1.5	550	90	529	0.31
9	1	450	30	599	0.33
10	2	450	30	705	0.4
11	1	450	90	876	0.496
12	2	450	90	698	0.39
13	1.5	450	60	403	0.25
14	1.5	450	60	427	0.25
15	1.5	450	60	374	0.21

Copyright © 2027, ISSN 1978-2993

respectively) indicate good agreement between the experimental and predicted values. The significance of the individual and interaction terms was evaluated, and terms with p-values lower than 0.05 were considered significant. Factors *A* and *B* were found to be non-significant for both responses and were therefore excluded from the models, whereas only the interaction between impregnation ratio and carbonization time (*AB*) was significant. In addition, the adequate precision values (15.5 for S_{BET} and 14.65 for V_P) were greater than 4, indicating an adequate signal-to-noise ratio and a good relationship between the experimental and calculated results. The low coefficients of variation (C.V. = 9.87% for S_{BET} and 10.46% for V_P) also confirm the reliability of the models for describing the process under study.

Figure 1 presents the regression plots of predicted versus actual values (*b*, *d*) and the normal probability plots of the residuals (*a*, *c*) for S_{BET} and V_P, respectively. The data points are distributed close to the diagonal line, indicating good agreement between the experimental and predicted values and confirming the adequacy of the quadratic models. In addition, the residuals follow an approximately straight line on the normal probability plots, indicating that they are normally distributed and that the assumption of normality underlying the ANOVA is satisfied. No obvious outliers or systematic deviations were observed, which suggests that the models adequately describe the relationship between the process variables and the responses.

One of the main advantages of RSM is that it allows the combined effects of the variables on the responses to be visualized in three-dimensional (3D) plots. Figure 2 (a) and (b) show the 3D plots of the interaction between impregnation ratio and carbonization time (*AB*)

Table 4. Analysis of variance (ANOVA) for the response model of BET surface area.

Source	Sum of squares	dF	Mean Square	F-value	p-value	
Model	4.525E5	9	50275.90	21.13	0.0018	Significant
A	37.91	1	37.91	0.0159	0.9045	
B	13068.92	1	13068.92	5.49	0.0661	
C	1.169E5	1	1.169E5	49.14	0.0009	
AB	20132.35	1	20132.35	8.46	0.0334	
AC	7797.86	1	7797.86	3.28	0.1300	
BC	14464.03	1	14464.03	6.08	0.0568	
A2	71039.62	1	71039.62	29.86	0.0028	
B2	1.186E5	1	1.186E5	49.83	0.0009	
C2	76378.82	1	76378.82	32.10	0.0024	
Residual	11896.29	5	2379.26			
Lack of Fit	10503.33	3	3501.11	5.03	0.1704	not significant
Pure Error	1392.96	2	696.48			
Cor. Total	4.644E5	14				
$R^2 = 0.9744$		$R_{adj}^2 = 0.9283$		$R_{pred}^2 = 0.6314$		

Table 5. Analysis of variance ANOVA for response model of total pore volume.

Source	Sum of squares	dF	Mean Square	F-value	p-value	
Model	0.1405	9	0.0156	18.32	0.0026	Significant
A	2.000E-0.6	1	2.000E-0.6	0.0023	0.9632	
B	0.0052	1	0.0052	6.11	0.0564	
C	0.0351	1	0.0351	41.22	0.0014	
AB	0.0077	1	0.0077	9.09	0.0296	
AC	0.0025	1	0.0025	2.93	0.1474	
BC	0.0035	1	0.0035	4.09	0.0992	
A2	0.0187	1	0.0187	21.95	0.0054	
B2	0.0341	1	0.0341	40.09	0.0014	
C2	0.0285	1	0.0285	33.44	0.0022	
Residual	0.0043	5	0.0009			
Lack of Fit	0.0032	3	0.0011	2.00	0.3511	not significant
Pure Error	0.0011	2	0.0005			
Cor Total	0.1447	14				
$R^2 = 0.9706$		$R_{adj}^2 = 0.9176$		$R_{pred}^2 = 0.6305$		

Copyright © 2027, ISSN 1978-2993

on the BET surface area and the total pore volume, respectively.

Although the individual effects of impregnation ratio (*A*) and carbonization time (*B*) were not statistically significant, their interaction (*AB*) had a significant influence on both responses. This indicates that the effect of one factor depends on the level of the other. As illustrated in Figure 2 (a) and (b), a low impregnation ratio combined with a long carbonization time was the most favorable combination. This suggests that a small amount of activating agent requires a longer time to develop the porosity, whereas an excess of agent promotes pore widening and partial collapse of the porous structure. In addition, the decrease in S_{BET} observed when the carbonization temperature increased beyond 450 °C can be attributed to several factors. At higher temperatures, the decomposition of volatile components and the softening of the char produce an intermediate melt within the char structure, which can lead to pore closure. At the same time, secondary volatiles continue to be released. The combination of pore closure by this intermediate melt and the further structural rearrangement of the char results in a lower BET surface area at higher carbonization temperatures [35].

The desirability function is employed for process optimization; it has values between 0 and 1. A value closer to 1 indicates higher reliability of the optimization. According to the data illustrated in Figure 3, the optimal conditions, with a desirability of 1, were identified for the maximum specific surface area and maximum total pore volume of the activated carbon. The identified optimal preparation parameters were a carbonization temperature of 450 °C, a time of 90 min, and an impregnation ratio of 1 w/w. The

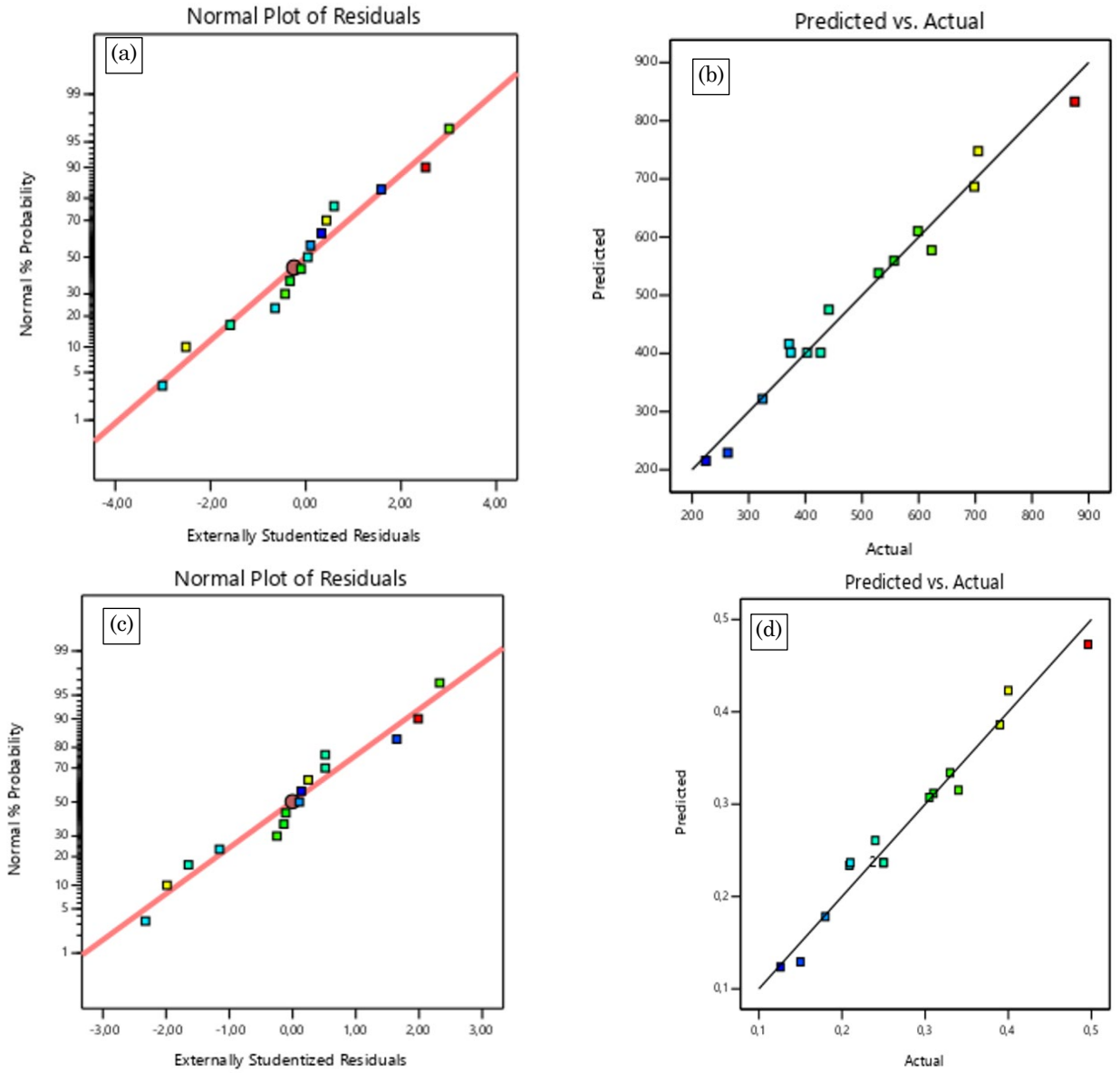


Figure 1. (b, d) Predicted versus actual values and (a, c) normal probability plots of the residuals for surface area and total pore volume.

Copyright © 2027, ISSN 1978-2993

model predicted the following optimal responses: a BET surface area of 833 m^2/g and a total pore volume of 0.473 cm^3/g. To validate these predictions, confirmatory experiments were carried out in triplicate under the optimal conditions. The experimental values of the BET surface area (873 m^2/g) and the total pore volume (0.490 cm^3/g) were in good agreement with the predicted ones, with relative errors of 4.6% and 3.47 % respectively, confirming the reliability and predictive capability of the quadratic models. The activated carbon prepared under these conditions was therefore selected for the adsorption experiments.

3.2. Characterization of the Biomass and Optimal Activated Carbon

3.2.1. Thermogravimetric analysis

The TGA/DTG thermal curves of the biomass and the optimal activated carbon are depicted in Figure 4. The thermal decomposition process of walnut shells is illustrated in Figure 4a. The raw material shows two noticeable stages of weight loss. The peak appearing between 200 °C and 400 °C is mainly linked to the breakdown of hemicellulose, cellulose, and lignin [36], with a mass loss of approximately 61%. The mass reduction between 400 °C and 1000 °C is due to the gasification of derivatized carbon precursors in the crystalline region [37], with a mass loss of approximately 13%. The thermal analysis of activated carbon is presented as a function of temperature in Figure 4b. The initial peak, observed between 30 °C and 100 °C, corresponds to the evaporation of water molecules within the sample, resulting in a mass loss of approximately 3% [38]. A further mass loss of around 20% was recorded in the temperature range of 200 °C to 900 °C. Additionally, a distinct peak appearing between 700 °C and 1000 °C is associated with the secondary devolatilization process, where

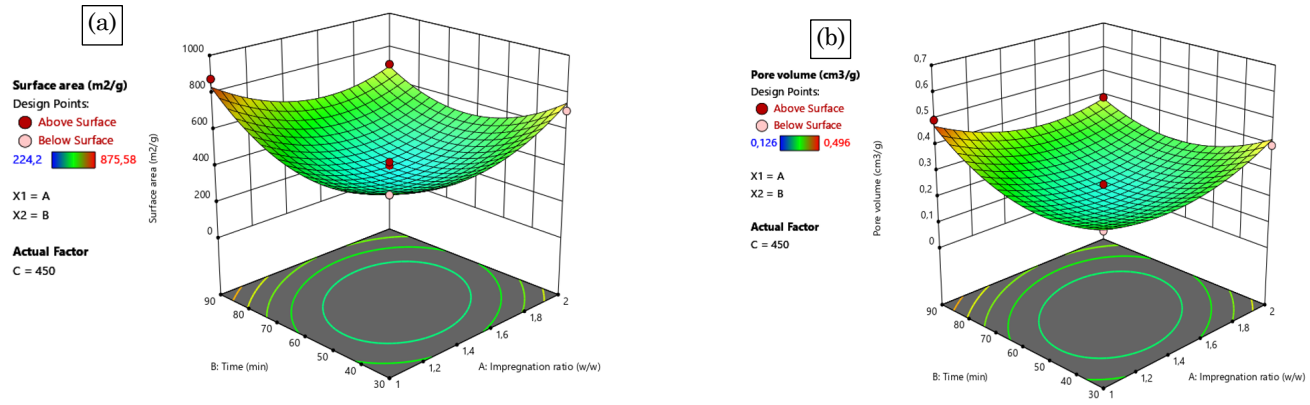


Figure 2. 3D surface plots for surface area and total pore volume responses for the effect of carbonization time and impregnation ratio.

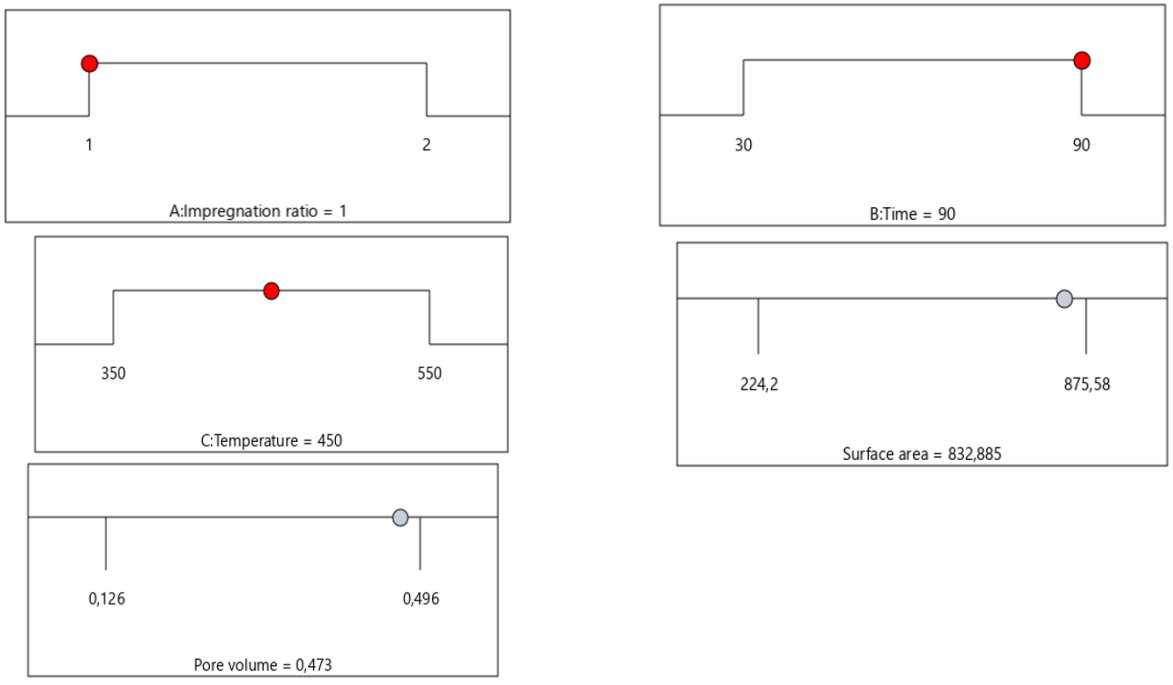


Figure 3. Optimal conditions for preparation of ACWS (Desirability = 1.000, Solution 11 out 100).

Copyright © 2027, ISSN 1978-2993

hydrogen and methane are released as the sample decomposes [39].

3.2.2. pH_{ZPC} analysis

In this study, 50 mL of a 0.1 M NaCl solution was introduced to separate beakers, and the pH of each solution was adjusted to values between 2 and 12. Subsequently, 0.05 g of activated carbon was added to each beaker and the mixtures were stirred for 48 hours. A control experiment without activated carbon was conducted simultaneously. After 48 hours, the pH of each solution was recorded, and the changes were plotted. The point at which the final pH intersected the initial pH was identified as the zero point charge (pH_{ZPC}) of the activated carbon. The pH_{ZPC} was determined to be 5.4 (Figure 5). This result suggests that the surface charge of the AC is neutral at pH of 5.4. Below this pH, the surface charge becomes positive, while above this pH, the ACWS surface acquires a negative charge.

3.2.3. BET analysis

The BET technique (Brunauer-Emmett-Teller) is instrumental for accurately characterizing the material's specific surface area. This is accomplished by quantifying the multilayer adsorption of high-purity nitrogen at a cryogenic temperature of 77 K, which is measured as a function of the relative pressure [40]. As evidenced in Figure 6a, the N_2 adsorption-desorption isotherm for the activated carbon, synthesized at a temperature of 450 °C, shows an uptake profile characteristic of microporous structures [41], particularly noticeable at lower relative pressures. Furthermore, adhering to the internationally recognized IUPAC classification, the shape of the adsorption-desorption curve clearly aligns with a Type IV isotherm, which is typically associated with materials exhibiting mesoporosity [32]. This mesoporous dominance is further supported by the pore size distribution (PSD) curve (Figure

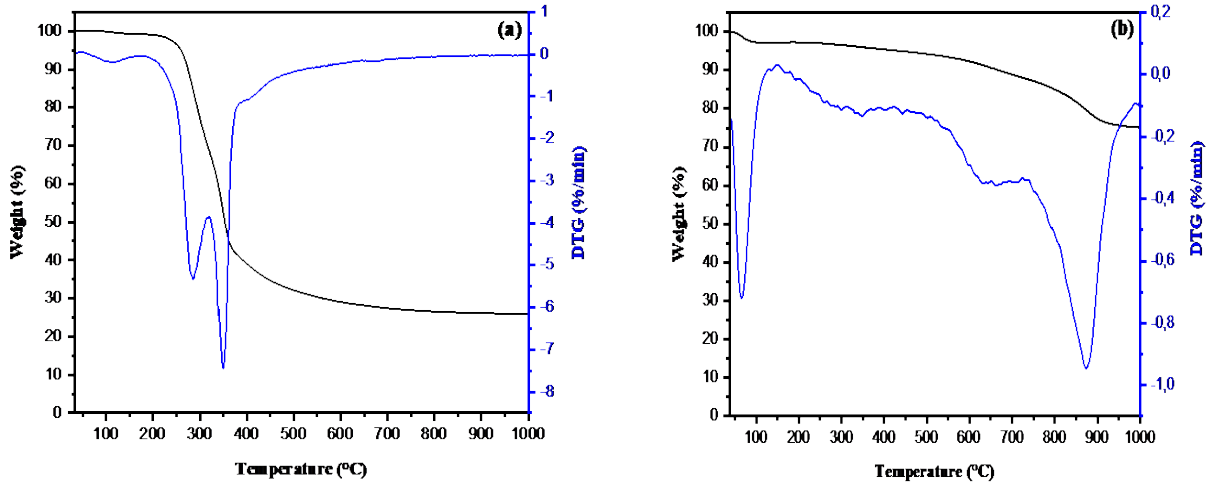


Figure 4. Thermogravimetric analysis of (a) raw material and (b) activated carbon.

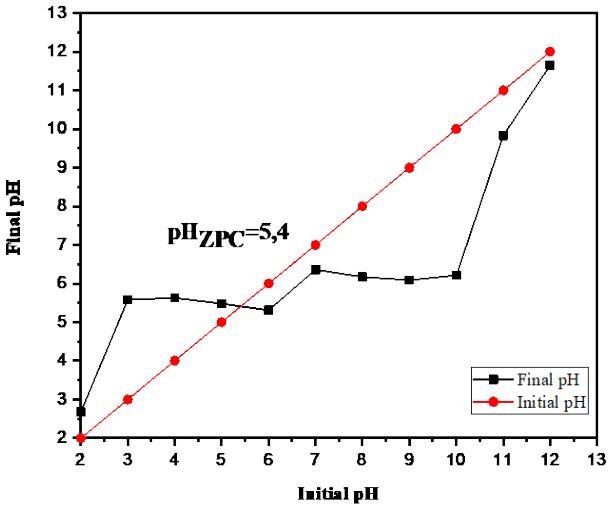


Figure 5. pH_{ZPC} of activated carbon.

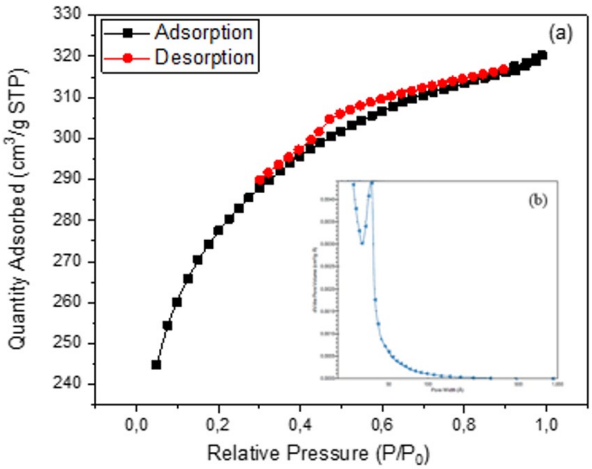


Figure 6. (a) Nitrogen adsorption-desorption isotherms of AC; (b) pore size distribution of AC.

Copyright © 2027, ISSN 1978-2993

6b), indicating that the sample's porosity is overwhelmingly composed of mesopores (2–50 nm), with only minor contributions from macropores (>50 nm) [42]. Quantification of the WSAC's porous metrics yielded the following detailed results: a BET surface area of 873 m^2/g, a total pore volume of 0.490 cm^3/g, and an average pore width of 2.85 nm.

3.2.4. SEM analysis

The surface morphology of the activated carbon prepared under optimal conditions was analyzed using scanning electron microscopy (SEM). The activated carbon from walnut shells displayed highly porous surfaces, resulting from the interaction between carbon and $ZnCl_2$. These interactions generated numerous mesopores, considerably increasing both the surface area and pore volume [43]. As illustrated in Figure 7, the activated carbon exhibited a variety of shapes and pore sizes. A significant portion of organic material was removed during the activation process, leading to pore formation [41]. Moreover, the external surface showed abundant cavities likely formed due to the release of chlorine gas and other volatile organic compounds during carbonization [38].

3.2.5. FTIR analysis

The FT-IR spectra of the walnut shell and the optimized activated carbon are presented in Figure 8. The spectrum of the raw material reveals the presence of several surface functional groups. The wide band at 3448 cm^{-1} was linked to O–H stretching from hydroxyl groups or adsorbed moisture, while the signal at 2926 cm^{-1} corresponds to C–H stretching in methyl and methylene groups [44]. The peak at 1743 cm^{-1} reflects the C=O stretching of aldehyde or ketone groups associated with hemicellulose. The band appearing 1510 cm^{-1} was characteristic of aromatic C–C stretching. The features at 1465 and 1428 cm^{-1} originate from C–H deformation modes [45]. Peaks found between 1378 and 1336

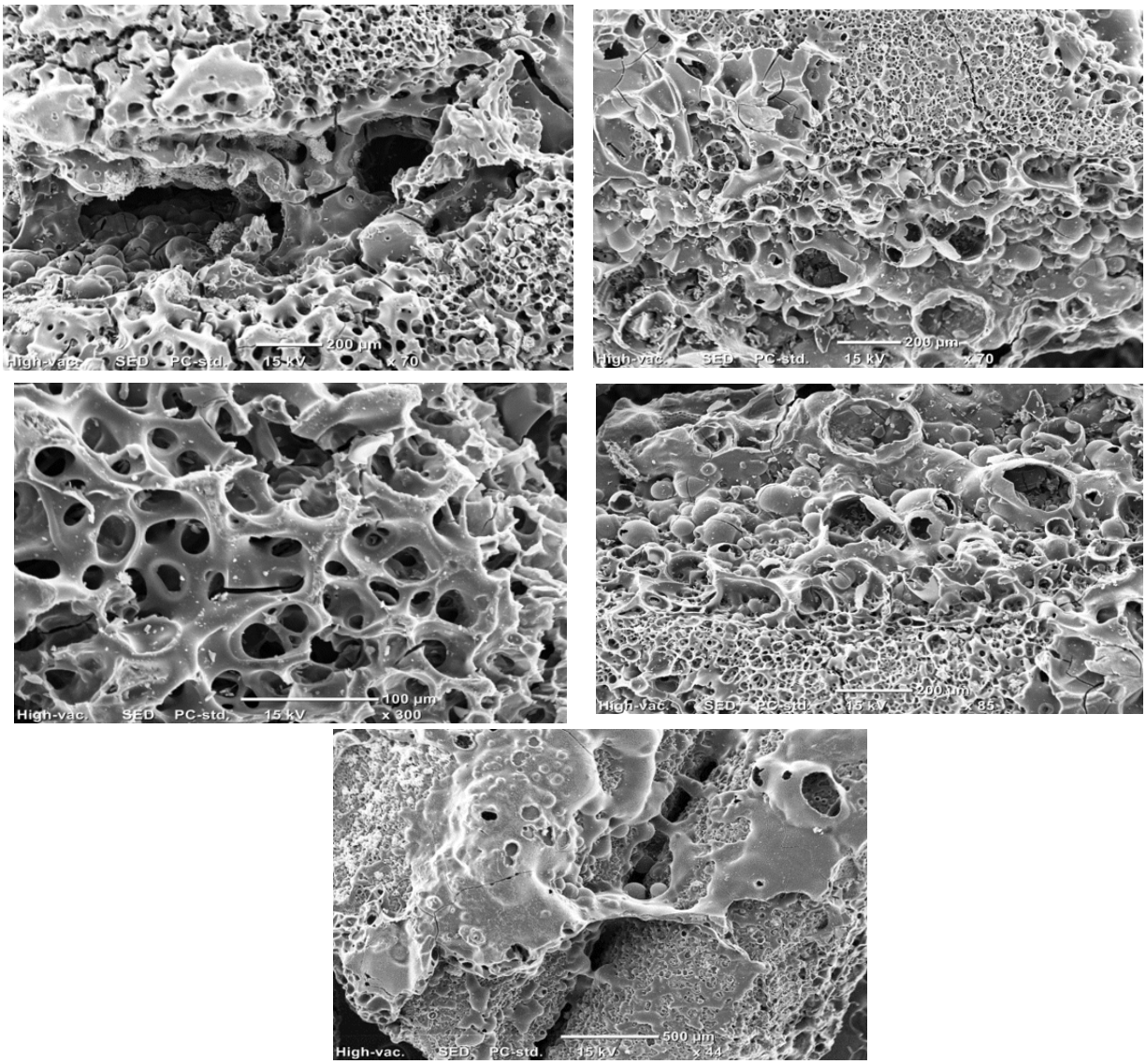


Figure 7. The scanning electron microscopy (SEM) of activated carbon.

Copyright © 2027, ISSN 1978-2993

cm^{-1} indicate carboxylic functionalities typically present in cellulose, lignin, and hemicellulose [46]. The signals at 1235 cm^{-1} and 1051 cm^{-1} arise from C–O stretching in alcohols, phenolic compounds, and ethers [47]. The weak peaks at 897 and 831 cm^{-1} are associated with C–H vibrations in benzene rings [44]. In contrast, the FT-IR spectrum of the activated carbon shows fewer functional groups, reflecting the decomposition of the precursor's surface functionalities during high-temperature pyrolysis. The band around 1582 cm^{-1} corresponds to C=C stretching [45], and the peaks detected in the 600–800 cm^{-1} region are attributed to out-of-plane C–H bending vibrations [41].

3.2.6. XRD analysis

The crystal phase composition of the walnut shell waste and the optimized activated carbon were determined via XRD (Figure 9). The precursor exhibited a semi-crystalline structure. The amorphous region was indicated by the broad reflection in the 2θ range spanning from 10° to 40°, which can be attributed to the lignin content present in the material [48]. The crystalline phase was associated with a peak observed at approximately 2θ = 22°, which can be attributed to the presence of crystalline cellulose in the biomass waste. This XRD diffraction pattern is commonly observed in lignocellulosic materials [45]. However, the XRD profile of the activated carbon shows only two typical peaks located at around 22.53° and 43.3°, attributed to the graphitic carbon crystal planes (002) and (100), respectively [49,50]. The weak, broad peaks indicated the amorphous nature of the activated carbon, which is composed of small domains formed by disordered graphene sheets, suggesting a low graphitic degree in the carbon [51]. Similar diffractograms of poorly crystalline carbon materials can be found in the following works [52, 53].

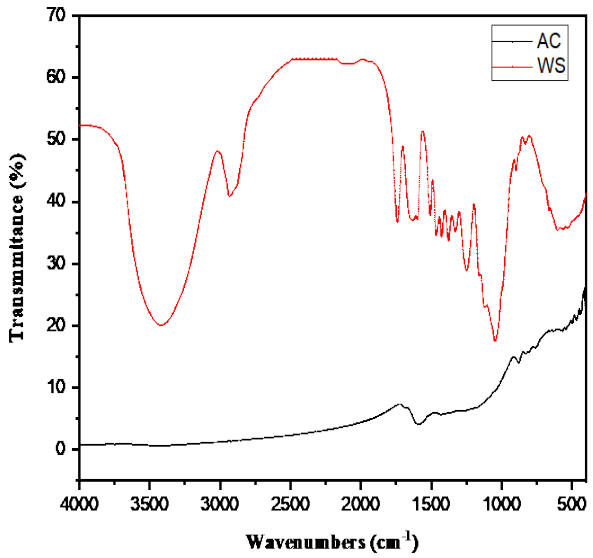


Figure 8. FTIR spectrum of precursor and activated carbon.

3.3. Adsorption Studies

3.3.1. Effect of pH

Paracetamol adsorption was investigated over a pH range of 3–12 using an initial PCT concentration of 20 $mg.L^{-1}$ and an activated carbon dosage of 1 $g.L^{-1}$, with a contact time of 4 h at ambient temperature. As illustrated in Figure 10A, the adsorption capacity remains nearly unchanged between pH of 3 and 9. Beyond pH of 9, a pronounced decline is observed, with the capacity decreasing from 17.78 to 10.3 $mg.g^{-1}$. This trend reflects the influence of solution pH on the surface charge of the adsorbent, driven by protonation in acidic media or hydroxide adsorption under alkaline conditions [53].

In acidic to neutral conditions, PCT exists predominantly in its neutral molecular form. Although the WSAC surface is positively charged below its pH_{ZPC} (5.4) and negatively charged above it, electrostatic interactions play a

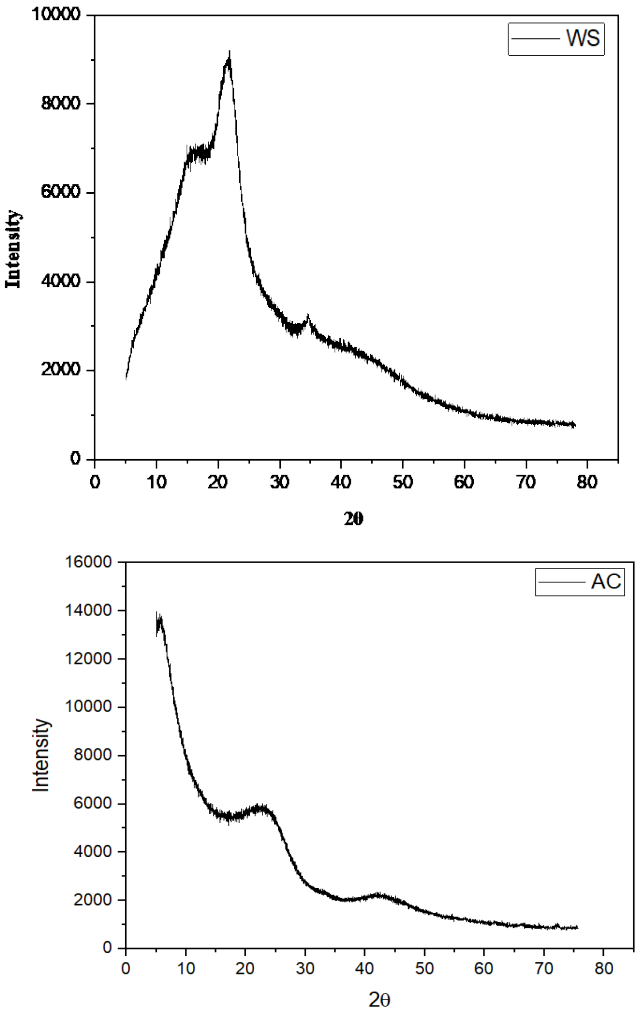


Figure 9. XRD patterns of walnut shell (WS) and activated carbon (AC).

Copyright © 2027, ISSN 1978-2993

negligible role owing to the uncharged nature of the PCT molecule. Instead, adsorption is mainly governed by non-electrostatic interactions, such as π–π electron donor-acceptor interactions between the aromatic ring of PCT and the graphitic basal planes of the adsorbent, and pore filling within the mesoporous structure of the activated carbon. Conversely, in strongly alkaline media (pH > pK_a 9.5), paracetamol undergoes deprotonation at its phenolic group, converting from its neutral form into its negatively charged anionic species [54]. Consequently, strong electrostatic repulsion occurs between the negatively charged WSAC surface and the anionic PCT molecules [55]. Furthermore, the high concentration of hydroxyl ions in alkaline solution exerts competitive adsorption for active surface sites.

3.3.2. Effect of adsorbent dose

The adsorption efficiency was evaluated by varying the adsorbent mass from 0.4 to 3 g.L^{-1} at an initial PCT concentration of 20 mg.L^{-1}, pH of 6, and a contact time of 4 h at room temperature. The results displayed that adsorption capacity (q_e) and removal efficiency (R) varied inversely (Figure 10B). The removal efficiency of PCT increased when the activated carbon dose was increased to 3 g.L^{-1}, with the adsorption rate increasing from 69.54 % to 94.71%. However, the adsorption capacity decreased from 34.77 to 6.31 mg.g^{-1}. Indeed, as an increase in the adsorbent dose increased the number of active sites, which led to greater PCT removal [56]. However, not all binding sites are readily accessible to the drug molecules, which leads to overlapping between the sites [57]. For this reason, the adsorption capacity of paracetamol decreased with increasing adsorbent dose. Based on the removal efficiency, the optimal dose of activated carbon was determined at 2 g.L^{-1}.

3.3.3. Effect of initial concentration of PCT

The influence of initial paracetamol concentration on adsorption capacity was evaluated by performing experiments at concentrations ranging from 20 to 50 mg.L^{-1}, at pH of 6 with an adsorbent dose of 2 g.L^{-1} and a constant temperature of 28 °C. As shown in Figure 10C, the maximum adsorption capacity

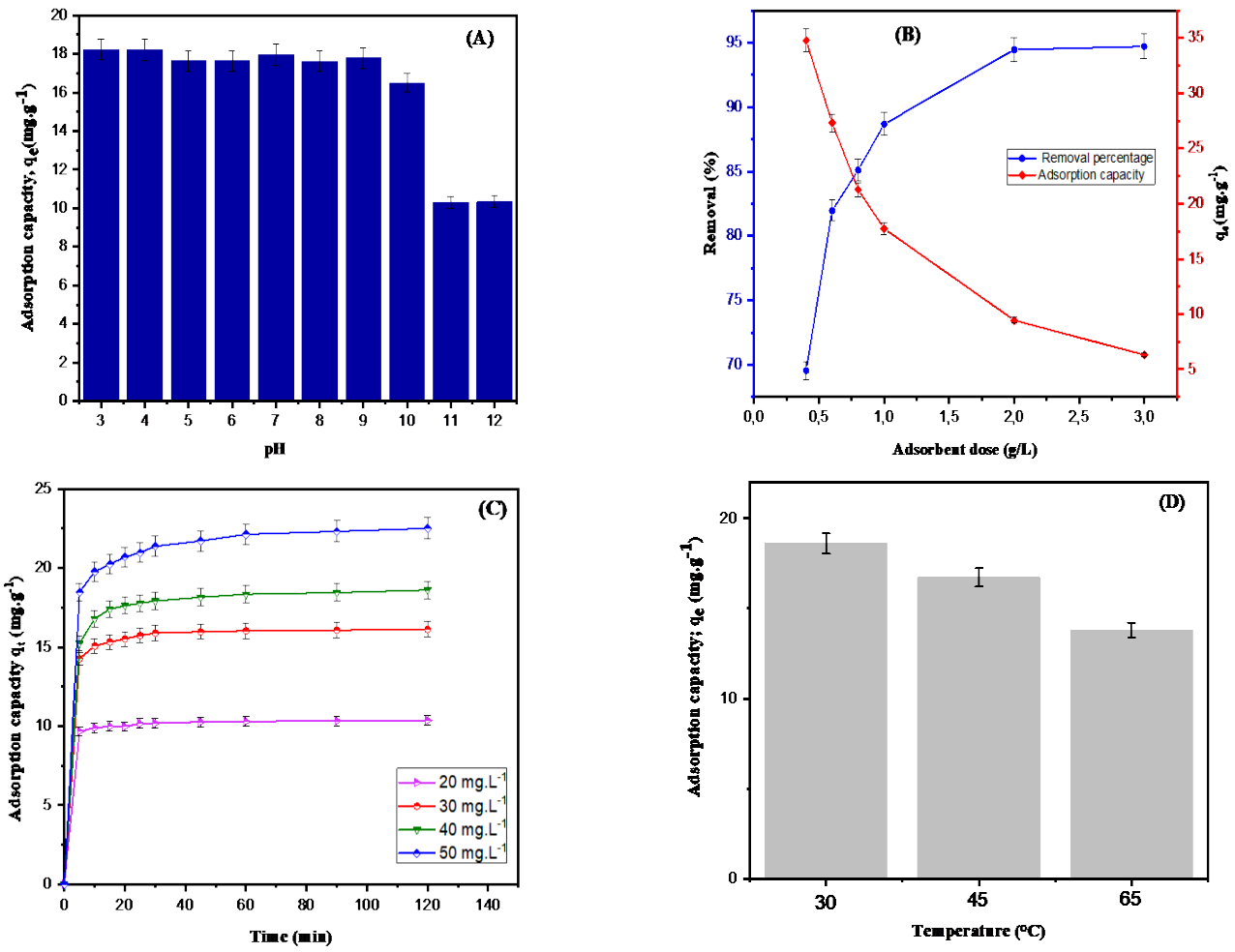


Figure 10. (A) Effect of initial pH on PCT adsorption capacity, (B) effect of adsorbent dose on PCT adsorption, (C) effect of initial concentration on PCT adsorption, (D) effect of solution temperature on paracetamol adsorption capacity by WSAC.

Copyright © 2027, ISSN 1978-2993

increased from 10.37 to 22.63 mg.g^{-1} with increasing initial concentration. During the first 20 minutes of the process, adsorption happens quickly. After that, the rate of adsorption progressively drops until equilibrium is reached. The high specific surface area and well-developed mesoporous structure of CACN, which offer numerous easily accessible active sites for PCT molecules, are responsible for this quick initial uptake. Higher starting concentrations also raise the concentration gradient, which serves as an encourage PCT mass transfer from the solution to the adsorbent surface.

3.3.4 Effect of temperature

The effect of temperature on PCT adsorption was investigated at three temperatures (30, 45, and 65 °C) under the optimal conditions, as shown in Figure 10D. At a WSAC dosage of 2 g.L^{-1}, a pH of 6 and an initial PCT concentration of 40 mg.L^{-1}, the adsorption capacity decreased from 18.61 mg.g^{-1} at 303 K to 13.8 mg.g^{-1} at 338 K after 45 min. This decrease with increasing temperature indicates that the adsorption process is exothermic. Similar trend was reported by Natarajan *et al.*, who observed reduced paracetamol adsorption at elevated temperatures of 303 to 317 K, indicating potential degradation of PCT at high temperatures [58].

3.3.5. Adsorption kinetic

In this work, several kinetic models have been proposed to study the mechanism of paracetamol adsorption such as the pseudo-first order, the pseudo second order, and the intraparticle diffusion. Table 6 presents the equations for the linear kinetic models, their parameters ($q_{e,cal}$, K_1 and K_2), and regression coefficients (R^2). The analysis of PFO parameters requires plotting ln ($q_e - q_t$) versus time (Figure 11 A). While the estimation of PSO parameters involves plotting t/q_t versus time (Figure 11 B). The intraparticle diffusion IPD model plot did not pass through the origin exhibiting a multilinear profile. This suggests that intraparticle diffusion represents only one stage of the adsorption process and is not the sole rate limiting step [12]. The kinetic parameters were determined by fitting the models under conditions of 40 mg.L^{-1} initial PCT concentration, pH of 6, an activated carbon dosage of 2 g.L^{-1}, and a temperature of 28 °C.

The PSO kinetic model yielded a higher determination coefficient (R^2 = 0.999) and a computed adsorption capacity that closely matched the experimental value, as indicated by the results displayed in Table 6. Historically, chemisorption involving electron sharing or exchange has been linked to a good fit to the PSO

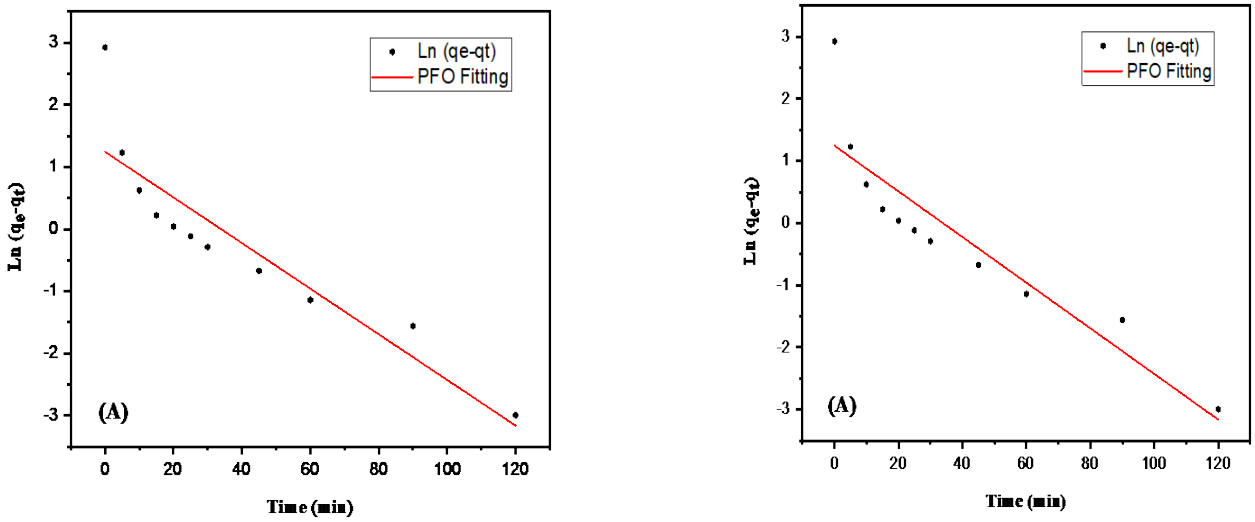


Figure 11. (A) The linear fitting of pseudo first-order and (B) pseudo second-order kinetic models.

Table 6. Parameters of the kinetic models.

Models	Pseudo-first-order			Pseudo-second-order		
Equations	$\ln(q_e - q_t) = \ln(q_e - K_1 t)$			$\frac{t}{q_e} = \frac{1}{K_2 q_e^2} + \frac{1}{q_e}$		
$q_{e,exp}$ (mg.g^{-1})	$q_{e,cal}$ (mg.g^{-1})	K_1 (min^{-1})	R^2	q_e,cal (mg.g^{-1})	K_2 (g.mg^{-1}.min^{-1})	R^2
18.66	17.45	0.0844	0.824	18.698	0.0509	0.9998

Copyright © 2027, ISSN 1978-2993

model. However, PSO is an empirical model by nature, reflecting the overall control of adsorption rate, which can also be driven by strong physical interactions instead of exclusive covalent bond formation, such as hydrogen bonding, electrostatic attraction, and π-π interaction [59].

3.3.6 Adsorption isotherm

The adsorption isotherm of PCT onto WSAC was determined at pH of 6, with an adsorbent dose of 2 $g.L^{-1}$ and a temperature of 30 °C (Figure 12). To describe the equilibrium data were fitted to the Langmuir and Freundlich models using nonlinear regression. Table 7 shows the calculated parameters and error analysis of the isotherms under study. With a maximum adsorption capacity (q_m) of 62.06 ± 5.87 $mg.g^{-1}$ and a Langmuir constant (K_L) of 0.155 ± 0.040 $L.mg^{-1}$ (95% confidence interval), the results indicated that the Langmuir model (R^2 = 0.995; SSE = 5.79) better described the experimental data than the Freundlich model (R^2 = 0.969; SSE = 37.00). The range of the dimensionless separation factor (R_L) was 0.244 to 0.047. These values, which are all between 0 and 1, verify that paracetamol adsorption onto WSAC is advantageous throughout the whole concentration range examined. Although a good fit by itself cannot prove surface homogeneity or the adsorption mechanism, this behavior is consistent with monolayer-type adsorption on a finite number of sites [55]. The value of n = 2.37 ± 0.71, which falls between 1 and 10, also suggests a favorable adsorption of paracetamol onto WSAC, despite the Freundlich model providing a less satisfactory fit.

3.3.7. Adsorption thermodynamic

The standard Gibbs free energy change (ΔG°) was calculated using Equation (13), whereas the standard enthalpy (ΔH°) and entropy (ΔS°) changes were determined from the slope and intercept, respectively, of the plot of ln (K_d) versus 1/T (Figure 13). The thermodynamic parameters are shown in Table 8. The negative ΔG° values confirm the spontaneous nature and thermodynamic feasibility of the adsorption process of PCT onto WSAC. It has been reported by several authors that the Gibbs free energy can estimate the type of adsorption, either chemisorption (-400 < ΔG° < -80 $kJ.mol^{-1}$) or physisorption (-20 < ΔG° < 0 $kJ.mol^{-1}$) [60,61]. Based on the data shown in Table 8, it appears that the mechanism of adsorption is governed predominantly physisorption with the possibility of stronger forces like hydrogen bonding and π-π

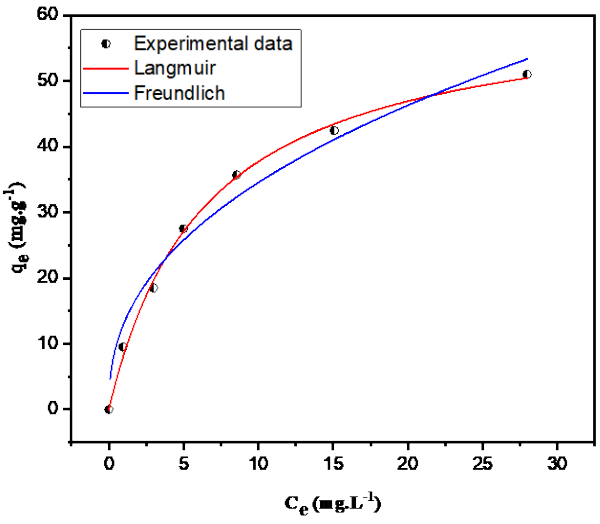


Figure 12. Langmuir and Freundlich adsorption isotherms.

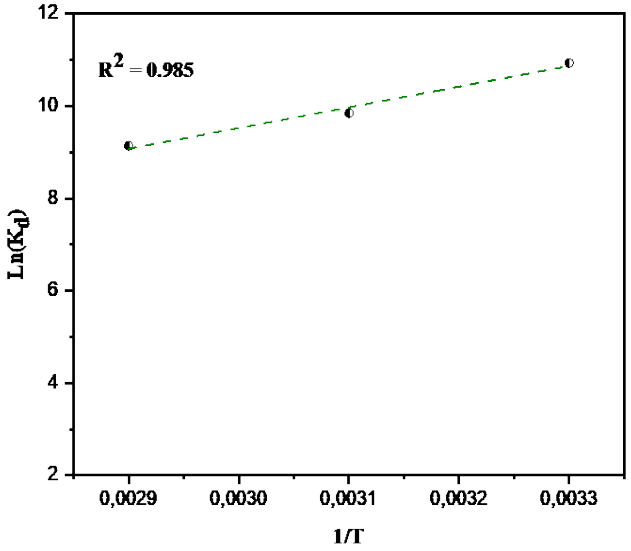


Figure 13. Van't Hoff plot for the adsorption of paracetamol onto WSAC.

Table 7. Nonlinear fitting parameters and error analysis of the Langmuir and Freundlich models for PCT adsorption onto WSAC.

Langmuir isotherm		Freundlich isotherm	
q_m (mg.g^{-1})	62.06 ± 5.87	K_F (mg$^{1-1/n}$.L$^{1/n}$.g^{-1})	13.065 ± 4.483
K_L (L.mg^{-1})	0.155 ± 0.040	n	2.37 ± 0.71
R^2	0.995	R^2	0.969
RMSE	0.983	RMSE	2.483
SSE	5.795	SSE	37.0
χ^2	0.460	χ^2	1.661

Copyright © 2027, ISSN 1978-2993

interactions. The negative value of ΔH° (-37.29 kJ.mol^{-1}) signifies that energy is released in the form of heat, which indicates the exothermic character of the adsorption process [62,63]. Furthermore, a decrease in randomness at the solid/liquid interface is indicated by the negative value of ΔS° (-32.68 J.mol^{-1}.K^{-1}), which is consistent with similar findings in research by Cazetta *et al.* [61].

3.3.8. Comparison study

A comparative evaluation of various activated carbons reported in the literature for paracetamol removal is summarized in Table 9. WSAC demonstrates a highly competitive adsorption capacity (q_m) compared to several carbons prepared from other precursors. These variations stem primarily from differences in experimental parameters across studies such as initial pH, temperature, adsorbent dosage, and initial PCT concentration, as well as distinct textural characteristics (specific surface area and total pore volume), synthesis protocols, and activation methods. Overall, WSAC, a low-cost adsorbent derived from walnut shell, exhibits a competitive adsorption capacity for the removal of PCT under the conditions studied.

4. Conclusions

This study presents an innovative approach for the valorization of walnut shells, an abundant agricultural waste, by converting them into high-performance activated carbon (WSAC) via chemical activation using $ZnCl_2$. The synthesis process was systematically optimized using Response Surface Methodology (RSM), which allowed precise determination of the optimal preparation conditions: 90 min, an impregnation ratio of 1 w/w, and a temperature of 450 °C. Under these conditions, WSAC exhibited exceptional physicochemical properties, including a high BET surface area of 873 m²/g and a total pore volume of 0.490 cm³/g, highlighting the efficiency of the activation process in generating a well-developed porous structure. The adsorption performance of WSAC was evaluated using paracetamol as a model pollutant. The material demonstrated remarkable removal efficiency, with an adsorption capacity of 18.66 mg.g^{-1} under an adsorbent dose of 2 g.L^{-1}, pH of 6, and an initial concentration of 40 mg.L^{-1} at room temperature. Importantly, the adsorption process remained stable across a broad pH range (3–9), indicating that WSAC can perform effectively under diverse water chemistries. Kinetic studies revealed that the adsorption followed a pseudo-second-order model, while equilibrium data were best described by the Langmuir isotherm ($R^2 = 0.995$), with a maximum adsorption capacity of 62.06 ± 5.87 mg.g^{-1}. Thermodynamic analysis further confirmed that the process is spontaneous and exothermic, reinforcing the material's suitability for practical water treatment applications. In the next phase of our work, we will focus on the regeneration and reusability of WSAC, on the environmental effects of $ZnCl_2$ activation, including the recovery or treatment of the Zn-containing washing solution, and an economic evaluation to assess large-scale applicability.

Table 9. Comparison of the maximum adsorption capacity of WSAC versus other adsorbents for PCT removal.

Adsorbent	q_m (mg.g^{-1})	References
RSAC	26.04	[64]
MSAC	11.47	[65]
HCAC	1.48	[66]
WD-Extra	29.3	[67]
PPAC	37.17	[68]
WSAC	15.90	[69]
WSAC	62.06	The present study

Acknowledgements

This work was supported by the Ministry of Higher Education and Scientific Research, Tunisia. Financial assistance was provided through the University of Gabes under the alternance scholarship program. The authors gratefully acknowledge the National Engineering School of Gabes (ENIG), University of Gabes, Tunisia, and the Department of Civil Engineering and Environment, IMT Lille Douai, LGCgE (EA 4515), University of Lille, F-59000 Lille, France, for hosting part of this research and providing access to their laboratory facilities.

Conflict of Interest

The authors declare that there are no conflicts of interest relevant to the content of this article.

Table 8. Thermodynamic parameters for PCT adsorption.

Temperature (K)	ΔG° (kJ.mol^{-1})	ΔH° (kJ.mol^{-1})	ΔS° (J.mol^{-1}.K^{-1})
303.15	-27.56		
318.15	-26.05	-37.29	-32.68
338.15	-25.70		

Copyright © 2027, ISSN 1978-2993

Funding

This work received no financial support from any organization.

Declaration of Generative AI Use

During the preparation of this revision, the author(s) did not use any generative AI or AI-assisted tools.

CRediT Author Statement

Author Contributions: Mariem Ouled Mohamed: conceptualization, methodology, writing - Original Draft, formal analysis, software, investigation, review and editing; Leila Khalfa: supervision, visualization, validation, writing, review and editing; Noureddine Hamdi: supervision, visualization, validation, investigation, review and editing; Mohamed Bagane: supervision, validation; Walid Maherzi: Funding acquisition, methodology investigation, review and editing. All authors have read and agreed to the published version of the manuscript.

References

[1] Archana, G., Dhodapkar, R., Kumar, A. (2017). Ecotoxicological risk assessment and seasonal variation of some pharmaceuticals and personal care products in the sewage treatment plant and surface water bodies (lakes). *Environmental Monitoring and Assessment*, 189(9), 446. DOI : 10.1007/s10661-017-6148-3.

[2] Mabalane, K., Thabede, P.M., Shooto, N.D. (2024). Removal of ibuprofen and paracetamol from water using a blend activated carbon from paper waste and avocado seeds. *Green Analytical Chemistry*, 10, 100135. DOI: 10.1016/j.greeac.2024.100135.

[3] Ayoub, S.S. (2021). Paracetamol (acetaminophen): A familiar drug with an unexplained mechanism of action. *Temperature*, 8(4), 351–371. DOI: 10.1080/23328940.2021.1886392.

[4] Kekes, T., Nika, M.-C., Tsopelas, F., Thomaidis, N.S., Tzia, C. (2020). Use of δ-manganese dioxide for the removal of acetaminophen from aquatic environment : Kinetic–thermodynamic analysis and transformation products identification. *Journal of Environmental Chemical Engineering*, 8(6), 104565. DOI: 10.1016/j.jece.2020.104565.

[5] Hamadneh, I., Abu-Zurayk, R.A., Aqel, A., Al-Mobydeen, A., Hamadneh, L., Al-Dalahmeh, Y., … Al-Dujaili, A.H. (2022). Impact of H3PO4-activated carbon from pine fruit shells for paracetamol adsorption from aqueous solution. *Desalination and Water Treatment*, 264, 293–306. DOI: 10.5004/dwt.2022.28589.

[6] Wu, S., Zhang, L., Chen, J. (2012). Paracetamol in the environment and its degradation by microorganisms. *Applied microbiology and Biotechnology*, 96(4), 875–884. DOI: 10.1007/s00253-012-4414-4.

[7] Rad, L.R., Haririan, I., Divsar, F. (2015). Comparison of adsorption and photo-Fenton processes for phenol and paracetamol removing from aqueous solutions: single and binary systems. *Spectrochimica Acta Part A: Molecular and Biomolecular Spectroscopy*, 136, 423–428. DOI: 10.1016/j.saa.2014.09.052.

[8] Pacheco-Álvarez, M., Benítez, R.P., Rodríguez-Narváez, O.M., Brillas, E., Peralta-Hernández, J.M. (2022). A critical review on paracetamol removal from different aqueous matrices by Fenton and Fenton-based processes, and their combined methods. *Chemosphere*, 303, 134883. DOI: 10.1016/j.chemosphere.2022.134883.

[9] Ntone, E.P.N., Abd Rahman, S., Samah, R.A., & Alsalhy, Q.F. (2024). Enhanced paracetamol removal using PES/GO mixed matrix membranes: A study on synthesis, characterization, and performance evaluation. *Journal of Engineering Research*. 13 (4), 2826-2838. DOI: 10.1016/j.jer.2024.11.011.

[10] Kouadio, K.E., Kambiré, O., Koffi, K.S., Ouattara, L. (2021). Electrochemical oxidation of paracetamol on boron-doped diamond electrode: Analytical performance and paracetamol degradation. *Journal of Electrochemical Science and Engineering*, 11(2), 71–86. DOI: 10.5599/jese.932.

[11] Gupta, S., Singh, A., Sharma, T., Kaur, R., Khandelwal, V., Rawat, K.D., … Shah, M.P. (2024). Applications of ultrafiltration, nanofiltration, and reverse osmosis in pharmaceutical wastewater treatment. In *Development in Wastewater Treatment Research and Processes* (pp. 33–49). Elsevier. DOI: 10.1016/b978-0-323-99278-7.00017-1.

[12] Macías-García, A., García-Sanz-Calcedo, J., Carrasco-Amador, J.P., Segura-Cruz, R. (2019). Adsorption of paracetamol in hospital wastewater through activated carbon filters. *Sustainability*, 11(9), 2672. DOI: 10.3390/su11092672.

[13] Doğan, E.C., Yaşar, A., Narcı, A.O., Mert, B.K., Yeşildağlı, B.U. (2025). Optimisation of nanofiltration process for pharmaceutically active compounds: Removal of paracetamol, diclofenac and metoprolol. *Water and Environment Journal*, 39(1), 5–19. DOI: 10.1111/wej.12954.

[14] Avramescu, S.M., Fierascu, I., Fierascu, R.C., Brazdis, R.I., Nica, A.V., Butean, C., … Dumitru, A. (2022). Removal of paracetamol from aqueous solutions by photocatalytic ozonation over TiO2-MexOy thin films. *Nanomaterials*, 12(4), 613. DOI: 10.3390/nano12040613.

[15] Peralta-Hernández, J.M., Brillas, E. (2023). A critical review over the removal of paracetamol (acetaminophen) from synthetic waters and real wastewaters by direct, hybrid catalytic, and sequential ozonation processes. *Chemosphere*, 313, 137411. DOI : 10.1016/j.chemosphere.2022.137411 .

Copyright © 2027, ISSN 1978-2993

[17] Spaltro, A., Pila, M.N., Colasurdo, D.D., Grau, E.N., Román, G., Simonetti, S., Ruiz, D.L. (2021). Removal of paracetamol from aqueous solution by activated carbon and silica. Experimental and computational study. *Journal of Contaminant Hydrology*, 236, 103739. DOI: 10.1016/j.jconhyd.2020.103739.

[18] Dávila-Estrada, M., Ramírez-García, J.J., Solache-Ríos, M.J., Gallegos-Pérez, J.L. (2018). Kinetic and equilibrium sorption studies of ceftriaxone and paracetamol by surfactant-modified zeolite. *Water, Air, & Soil Pollution*, 229(4), 123. DOI: 10.1007/s11270-018-3783-4.

[19] Saha, B., Gayen, S., Debnath, A. (2023). Sequestration of paracetamol from aqueous solution using zinc oxide/polypyrrole nanocomposite: cost analysis, scale-up design, and optimization of process parameters. *Journal of Hazardous, Toxic, and Radioactive Waste*, 27(4), 04023032. DOI: 10.1061/jhtrbp.hzeng-1213.

[20] Fuentes, A.L.B., Canevesi, R.L.S., Gadonneix, P., Mathieu, S., Celzard, A., Fierro, V. (2020). Paracetamol removal by Kon-Tiki kiln-derived biochar and activated carbons. *Industrial Crops and Products*, 155, 112740. DOI: 10.1016/j.indcrop.2020.112740.

[21] Ferreira, R.C., de Araújo, T.P., Dias, D., Bernardo, M., Lapa, N., Fonseca, I.M., de Barros, M.A.S.D. (2023). Removal of paracetamol and Cu2+ from water by using porous carbons derived from agrowastes. *Processes*, 11(7), 2146. DOI: 10.3390/pr11072146.

[22] Mahmoudi, K, Hamdi, N, Ali, MB, Jellali, S., Srasra, E. (2020). Enhanced adsorptive removal of cationic and anionic dyes from aqueous solutions by olive stone activated carbon. *Comptes Rendus Chimie*, 23 (11-12), 689-704. DOI: 10.5802/crchim.54.

[23] Amri, I., Assadi, A.A., Mellah, B., Hamdi, N. (2024) Optimized removal of chloroform and DMDS using synthetic zeolite (Na-P1) and activated carbon composite, *Modeling Earth Systems and Environment*, 10(2), 2309–2328. DOI: 10.1007/s40808-023-01911-2.

[24] Hamdi, W., Hamdi, N., Jellali, S., Jeguirim, M., Seffen, M., (2023) Investigations on phosphorus recovery characteristics by active carbon prepared from date stones in aqueous solutions. *Desalination and Water Treatment.* 282, 212–219, DOI: 10.5004/dwt.2023.29165

[25] Teimouri, Z., Salem, A., Salem, S. (2019). Microwave-assisted for clean and rapid fabrication of highly efficient magnetically separable activated carbon from agriculture shells for low grade industrial corn syrup decoloration: A novel strategy for impregnation of ternary catalytic composite. *Food and Bioproducts Processing*, 116, 78–88. DOI : 10.1016/j.fbp.2019.04.013 .

[26] Rawat, S., Singh, J. (2021). Green synthesis of iron nanoparticles using Plumeria and Jatropha: characterization and investigation of their adsorption, regeneration and catalytic degradation efficiencies. *BioNanoScience*, 11(4), 1142–1153. DOI: 10.1007/s12668-021-00894-7 .

[27] Musah, M., Azeh, Y., Mathew, J., Umar, M., Abdulhamid, Z., Muhammad, A. (2022). Adsorption kinetics and isotherm models: a review. *Caliphate Journal of Science and Technology*, 4(1), 20–26. DOI: 10.4314/cajost.v4i1.3.

[28] Lima, E.C., Sher, F., Guleria, A., Saeb, M.R., Anastopoulos, I., Tran, H.N., Hosseini-Bandegharaei, A. (2021). Is one performing the treatment data of adsorption kinetics correctly? *Journal of Environmental Chemical Engineering*, 9(2), 104813. DOI: 10.1016/j.jece.2020.104813.

[29] Jawad, A.H., Surip, S.N. (2022). Upgrading low rank coal into mesoporous activated carbon via microwave process for methylene blue dye adsorption: Box Behnken Design and mechanism study. *Diamond and Related Materials*, 127, 109199. DOI: j.diamond.2022.109199.

[30] Yahya, K., Ba, M., Msadok, I., Mlayah, A., Srasra, E., Hamdi, N. (2022). Removal of phosphate from synthetic wastewater: A comparative study between both activated clays using an experimental design methodology. *Water Environment Research*, 94(11), e10800. DOI: 10.1002/wer.10800.

[31] Abderrahim, N., Mergbi, M., Amor, H. Ben, Djellabi, R. (2023). Optimization of microwave assisted synthesis of activated carbon from biomass waste for sustainable industrial crude wet-phosphoric acid purification. *Journal of Cleaner Production*, 394, 136326. DOI: 10.1016/j.jclepro.2023.136326.

[32] Qadri, T., Naik, H.R., Hussain, S.Z., Bhat, T.A., Naseer, B., Zargar, I., Beigh, M.A. (2023). Impact of spray drying conditions on the reconstitution, efficiency and flow properties of spray dried apple powder-optimization, sensorial and rheological assessment. *Heliyon*, 9(8). DOI: 10.1016/j.heliyon.2023.e18527.

[33] Shabir, S., Hussain, S.Z., Bhat, T.A., Amin, T., Beigh, M., Nabi, S. (2024). High carbon content microporous activated carbon from thin walnut shells: Optimization, physico-chemical analysis and structural profiling. Process Safety and Environmental Protection, 190, 85–96. DOI : 10.1016/j.psep.2024.06.121 .

[34] Zhang, Y., Yang, H., Wang, B., Khan, H.M.S., Duan, X., Liu, Y. (2022). Morphology structure evolution and combustion reactivity of bituminous char at around ash melting temperature. *Journal of Thermal Science*, 31(6), 2189–2202. DOI: 10.1007/s11630-022-1686-6.

Copyright © 2027, ISSN 1978-2993

[35] Pan, F., Wei, H., Huang, Y., Song, J., Gao, M., Zhang, Z., … Jing, S. (2024). Phosphorus adsorption by calcium chloride-modified buckwheat hulls biochar and the potential application as a fertilizer. *Journal of Cleaner Production*, 444, 141233. DOI: 10.1016/j.jclepro.2024.141233.

[36] Nguyen, V.-T., Nguyen, T.-B., Huang, C.P., Chen, C.-W., Bui, X.-T., Dong, C.-D. (2021). Alkaline modified biochar derived from spent coffee ground for removal of tetracycline from aqueous solutions. *Journal of Water Process Engineering*, 40, 101908. DOI: 10.1016/j.jwpe.2020.101908.

[37] Mohseni, E., Rahmani, A., Hamdi, Z., Ghorbanzadeh, P. (2024). Efficiency of response surface method based on central composite design in optimizing the adsorption process of cadmium metal from aqueous solutions using activated charcoal prepared from walnut shell. *Desalination and Water Treatment*, 317, 100250. DOI: 10.1016/j.dwt.2024.100250.

[38] Goscianska, J., Nowicki, P., Nowak, I., Pietrzak, R. (2012). Thermal analysis of activated carbons modified with silver metavanadate. *Thermochimica Acta*, 541, 42–48. DOI: 10.1016/j.tca.2012.04.026.

[39] Ren, Y., Cui, M., Zhou, Y., Lee, Y., Ma, J., Han, Z., Khim, J. (2023). Zero-valent iron based materials selection for permeable reactive barrier using machine learning. *Journal of Hazardous Materials*, 453, 131349. DOI: 10.1016/j.jhazmat.2023.131349.

[40] Serafin, J., Dziejarski, B., Junior, O.F.C., Sreńscek-Nazzal, J. (2023). Design of highly microporous activated carbons based on walnut shell biomass for H2 and CO2 storage. *Carbon*, 201, 633–647. DOI: 10.1016/j.carbon.2022.09.013.

[41] Tella, J.O., Adekoya, J.A., Ajanaku, K.O. (2022). Mesoporous silica nanocarriers as drug delivery systems for anti-tubercular agents: a review. *Royal Society Open Science*, 9(6), 220013. DOI: 10.1098/rsos.220013.

[42] Cheng, S., Zhang, L., Xia, H., Peng, J., Zhang, S., Wang, S. (2015). Preparation of high specific surface area activated carbon from walnut shells by microwave-induced KOH activation. *Journal of Porous Materials*, 22(6), 1527–1537. DOI: 10.1007/s10934-015-0035-5.

[43] Yang, J., Qiu, K. (2010). Preparation of activated carbons from walnut shells via vacuum chemical activation and their application for methylene blue removal. *Chemical Engineering Journal*, 165(1), 209–217. DOI: 10.1016/j.cej.2010.09.019.

[44] Li, Z., Hanafy, H., Zhang, L., Sellaoui, L., Netto, M.S., Oliveira, M.L.S., … Li, Q. (2020). Adsorption of congo red and methylene blue dyes on an ashitaba waste and a walnut shell-based activated carbon from aqueous solutions: Experiments, characterization and physical interpretations. *Chemical Engineering Journal*, 388, 124263. DOI: 10.1016/j.cej.2020.124263.

[45] Banerjee, M., Basu, R.K., Das, S.K. (2018). Cr (VI) adsorption by a green adsorbent walnut shell: adsorption studies, regeneration studies, scale-up design and economic feasibility. *Process Safety and Environmental Protection*, 116, 693–702. DOI: 10.1016/j.psep.2018.03.037.

[46] Liu, G., Zhang, W., Luo, R. (2019). Synthesis, characterization of amino-modified walnut shell and adsorption for Pb (II) ions from aqueous solution. *Polymer Bulletin*, 76(3), 1099–1114. DOI: 10.1007/s00289-018-2424-9.

[47] Georgin, J., da Silva Marques, B., da Silveira Salla, J., Foletto, E.L., Allasia, D., Dotto, G.L. (2018). Removal of Procion Red dye from colored effluents using H2SO4-/HNO3-treated avocado shells (Persea americana) as adsorbent. *Environmental Science and Pollution Research*, 25(7), 6429–6442. DOI: 10.1007/s11356-017-0975-1.

[48] Albatrni, H., Abou Elezz, A., Elkhatat, A., Qiblawey, H., Almomani, F. (2024). A green route to the synthesis of highly porous activated carbon from walnut shells for mercury removal. *Journal of Water Process Engineering*, 58, 104802. DOI: 10.1016/j.jwpe.2024.104802.

[49] Husain, A., Ansari, K., Mahajan, D.K., Kandasamy, M., Ansari, M.N.M., Giri, J., Al-Lohedan, H.A. (2024). Harnessing sustainable N-doped activated carbon from walnut shells for advanced all-solid-state supercapacitors and targeted Rhodamine B dye adsorption. *Journal of Science: Advanced Materials and Devices*, 9(2), 100699. DOI: 10.1016/j.jsamd.2024.100699.

[50] Mallesh, D., Anbarasan, J., Kumar, P.M., Upendar, K., Chandrashekar, P., Rao, B., Lingaiah, N. (2020). Synthesis, characterization of carbon adsorbents derived from waste biomass and its application to CO2 capture. *Applied Surface Science*, 530, 147226. DOI: 10.1016/j.apsusc.2020.147226.

[51] Zhang, R., Qiao, J., Zhang, X., Yang, Y., Zheng, S., Li, B., … Zeng, Z. (2022). Biomass-derived porous carbon for microwave absorption. *Materials Chemistry and Physics*, 289, 126437. DOI: 10.1016/j.matchemphys.2022.126437.

[52] Abderrahim, N., Boumnijel, I., Amor, H. Ben, Djellabi, R. (2022). Heat and ZnCl2 chemical carbonization of date stone as an adsorbent: optimization of material fabrication parameters and adsorption studies. *Environmental Science and Pollution Research*, 29(30), 46038–46048. DOI: 10.1007/s11356-022-19132-y.

[53] Ramli, M.R.M., Shoparwe, N.F., Ahmad, M. A., & Yusop, M. F. M. (2024). Acetaminophen removal using porous activated carbon derived from corn cob: optimization and mass transfer modelling. Journal of Chemical Technology & Biotechnology, 99(9), 2088–2106. DOI: doi.org/10.1002/jctb.7712.

Copyright © 2027, ISSN 1978-2993

[54] Spessato, L., Bedin, K.C., Cazetta, A.L., Souza, I.P.A.F., Duarte, V.A., Crespo, L.H.S., … Almeida, V.C. (2019). KOH-super activated carbon from biomass waste: Insights into the paracetamol adsorption mechanism and thermal regeneration cycles. *Journal of Hazardous Materials*, 371, 499–505. DOI: 10.1016/j.jhazmat.2019.02.102.

[55] Yahia, E.H., Cherif, E.K., Ouzzine, M., Touijer, A., Coren, F., Saidi, M. (2023). Promising porous carbon material derived from argan paste cake by KOH activation, for paracetamol removal. *Processes*, 11(7), 2078. DOI: 10.3390/pr11072078.

[56] Sajid, M., Bari, S., Rehman, M.S.U., Ashfaq, M., Guoliang, Y., Mustafa, G. (2022). Adsorption characteristics of paracetamol removal onto activated carbon prepared from Cannabis. *Alexandria Engineering Journal*, 61, 7203–7212. DOI: 10.1016/j.aej.2021.12.060.

[57] Natarajan, R., Venkataraman, S., Rajendran, D. S., Tamilselvam, B., Zaveri, H., Jeyachandran, N., … Vaidyanathan, V.K. (2022). Adsorption performance of magnetic mesoporous silica microsphere support toward the remediation of acetaminophen from aqueous solution. *Journal of Water Process Engineering*, 48, 102835. DOI: 10.1016/j.jwpe.2022.102835.

[58] Maneewong, Y., Chaemchuen, S., Verpoort, F., Klomkliang, N. (2022). Paracetamol removal from water using N-doped activated carbon derived from coconut shell: Kinetics, equilibrium, cost analysis, heat contributions, and molecular-level insight. *Chemical Engineering Research and Design*, 185, 163–175. DOI: 10.1016/j.cherd.2022.07.007.

[59] Guedidi, H., Reinert, L., Soneda, Y., Bellakhal, N., Duclaux, L. (2017). Adsorption of ibuprofen from aqueous solution on chemically surface-modified activated carbon cloths. *Arabian Journal of Chemistry*, 10, S3584–S3594. DOI: 10.1016/j.arabjc.2014.03.007.

[60] Cazetta, A.L., Martins, A.C., Pezoti, O., Bedin, K.C., Beltrame, K.K., Asefa, T., Almeida, V.C. (2016). Synthesis and application of N–S-doped mesoporous carbon obtained from nanocasting method using bone char as heteroatom precursor and template. *Chemical Engineering Journal*, 300, 54–63. DOI: 10.1016/j.cej.2016.04.124.

[61] Alakayleh, Z. (2025). Sulfuric acid-activated carbon from guava leaves for paracetamol adsorption. *Results in Engineering*, 25, 103685. DOI: 10.1016/j.rineng.2024.103685.

[62] Igwegbe, C.A., Aniagor, C.O., Oba, S.N., Yap, P.-S., Iwuchukwu, F.U., Liu, T., … Ighalo, J.O. (2021). Environmental protection by the adsorptive elimination of acetaminophen from water: a comprehensive review. *Journal of Industrial and Engineering Chemistry*, 104, 117–135. DOI: 10.1016/j.jiec.2021.08.015.

[63] Çifçi, D.İ. (2024). Diclofenac sodium and paracetamol removal with ZnCl2 activated carbon produced from rice straw. *International Journal of Phytoremediation*, 26(11), 1847–1853. DOI: 10.1080/15226514.2024.2357644.

[64] Preglo, A.R., Namata, J., Caculba, J., Sanchez, G., Joyno, C., Pagalan, E., Arazo, R.O. (2023). Paracetamol removal from aqueous solution through activated carbon from mango seeds. *Chemistry Africa*, 6(2), 699–710. DOI: 10.1007/s42250-023-00597-4.

[65] Parus, A., Gaj, M., Karbowska, B., Zembrzuska, J. (2020). Investigation of acetaminophen adsorption with a biosorbent as a purification method of aqueous solution. *Chemistry and Ecology*, 36(7), 705–725. DOI: 10.1080/02757540.2020.1757081.

[66] Skwarczynska-Wojsa, A. Puszkarewicz, A. (2024). Removal of Acetaminophen from Aqueous Solutions in an Adsorption Process. *Materials*, 17(2), 431. DOI: 10.3390/ma17020431.

[67] Turkmen Koc, S.N., Kipcak, A.S., MoroydorDerun, E., Tugrul, N. (2021). Removal of zinc from wastewater using orange, pineapple and pomegranate peels. *International Journal of Environmental Science and Technology*, 18(9), 27812792. DOI: 10.1007/S13762-020 03025-Z.

[68] Tunç Sara, M., Yıldız, B., Taşar, Ş. (2021). Removal of paracetamol from aqueous solution by wood sawdust-derived activated carbon: Process optimization using response surface methodology. *Chemical Engineering Communications*, 209(8), 1130–1150. DOI: 10.1080/00986445.2021.1978075.

[69] Aydin, S., Celik Karakaya, M., Karakaya, N., Aydin, M.E. (2023). Effective removal of selected pharmaceuticals from sewerage treatment plant effluent using natural clay (Na-montmorillonite). *Applied Water Science*, 13(6), 129. DOI: 10.1007/s13201-023-01930-5

Copyright © 2027, ISSN 1978-2993